PHYSICAL REVIEW E **93**, 042704 (2016)

# Ferrielectricity in smectic-$C^*$ dechiralization-line lattices

B. Mettout,[1] H. Pasco Logbo,[1,2] Y. Gagou,[3] H. Vasseur,[1] and P. Gisse[1]
[1] *PSC, Université de Picardie, 33 Rue Saint Leu, Amiens, France*
[2] *Faculté des Sciences et Techniques de Natitingou, USATN, Natitingou, Benin*
[3] *LPMC, Université de Picardie, 33 Rue Saint Leu, Amiens, France*

(Received 21 December 2015; revised manuscript received 15 February 2016; published 15 April 2016)

Recent experiments probing a new ferroelectric liquid crystal (CLF08) confined in cells with planar alignment have shown dielectric and optic anomalies suggesting the onset of ferrielectric ordering within the surface lattice of dechiralization lines. We present a phenomenological theory describing the corresponding phase transition sequence Sm$A \rightarrow$ Sm$C^* \rightarrow$ Ferri. Phase diagrams and thermodynamic, dielectric, and optic properties are worked out and compared with experiments. The anomalies are related to the predicted tristability of the experimental cells under applied electric field. The order parameters of Landau theory are reinterpreted in terms of line positions, allowing description of the entrance and exit line behavior, and yielding the prediction and identification of new *limit* phases within a nonconventional Landau approach.

DOI: 10.1103/PhysRevE.93.042704

## I. INTRODUCTION

Bulk and confined properties of chiral Sm$C^*$ liquid crystals [1–4] have been widely studied since their discovery in the mid-1970's. They are characterized by their ferroelectric properties at the molecular scale. Although bulk Sm$C^*$ exhibits an exact helielectric structure [5,6], in a thin cell with planar geometry, the continuous helical symmetry is broken by the presence of the cell walls, and the structure actually becomes antiferroelectric at the micron scale. This phenomenon is straightforward from the symmetry point of view, and can be more concretely described in terms of dechiralization lines: The cell walls force the bulk helix to unwind in their vicinity, so that one-dimensional lattices of linear defects appear close to the surfaces in order to protect the helix against the wall unwinding forces. On each side of the sample the distance between two adjacent lines is given by the helix pitch $\lambda$. These dechiralization lines [7–9] are positively charged $2\pi$ disclinations of the molecular tilt and polarization fields, which are represented by dots in Fig. 1. Their strong coupling with the applied electric field yields their large contribution to dielectric properties of the sample [10,11], and, in particular, to the field-induced unwinding transition [12,13] of the bulk helix. At zero applied electric field the lines are located at the same distance of the walls on both sides of the sample, so that their antiferroelectric character becomes clearly apparent: Polarization vectors connecting the negatively charged surfaces to the positive lines alternate periodically along the lattice.

These defects have been observed and described in smectic-$C$ samples for more than three decades (though their interpretation is not yet universally accepted [14]), whereas the antiferroelectric behavior is evidenced in dielectric measurements [5] by the presence of hysteresis loops of the polarization and permittivity versus electric field curves exhibiting two typical symmetrical lobes [15,16]. Such behavior has been recently confirmed [17,18] in a new ferroelectric liquid crystal (CLF08 with [1,1′-Biphenyl]-4-carboxylic acid, 4′-[[4[[6[(2cyanoacetyl) oxy]hexyl] oxy] benzoyl] oxy]-,1-methylheptyl ester chemical nomenclature) [19] synthesized by Dabrowski's group at the Institute of Chemistry, Military University of Technology (Poland), together with a number of anomalous behaviors.

Figure 2 presents the real part $\varepsilon'$ of the dielectric permittivity versus dc bias voltage in CLF08. The presence of two symmetric lobes gives the hysteresis curve a typical butterfly shape characteristic of antiferroelectric or helielectric materials. The unwinding transition is revealed by a drastic decay of $\varepsilon'$ above a critical field. The field hysteresis proves its first-order character.

However, a first anomaly can be seen on this curve: One observes a spectacular difference between the first polarization curve and the cycle. At zero field just after cooling, the permittivity is higher than at the end of the cycle at the same field. Accordingly, there exist two distinct zero-field states; the first is stabilized when the system is cooled at zero field, and the second is stabilized when the system has been previously submitted to field cycling. The persistency of the hysteresis down to zero field characterizes the second anomaly. It can be seen clearly on the left-hand part of the cycle presented in Fig. 2 as a triangle ending at zero. It becomes more pronounced at lower frequencies.

The third anomaly appears as a sharp increase of $\varepsilon'$ just before the unwinding transition ($-E10$ in Fig. 2). The corresponding maximum of $\epsilon'$ becomes stronger at higher frequencies. We interpret this maximum as the trace of a divergence onset characteristic of susceptibility in macroscopically ferroelectric systems, which is usually absent in antiferroelectrics or helielectrics.

Note that optic counterparts accompany these dielectric anomalies. The dechiralization lines are easily observed using a polarized light microscope, under crossed analyzer and polarizer. Their behavior during the field cycle, which follows precisely the changes in dielectric properties, will be presented and discussed in Sec. III. Reference [20] is devoted to an analysis of the interactions between the helix, lines, surface charge, and fields.

Finally, a fourth anomaly is observed in polarization versus field $P(E)$ hysteresis loops presented in Fig. 3 for various frequencies. Their shapes change from one-loop curves, typical in macroscopic ferroelectrics [21], to two juxtaposed high-field lobes connected by a central lobe. The two first

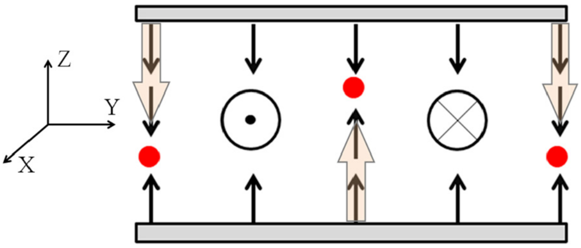

FIG. 1. Scheme of the polarization field in a Sm$C$* cell. Black thin arrows and large open circles represent the local in-plane ($zy$) polarization and large open circles represent the local out-of-plane ($x$) polarization. Small solid circles represent cuts of the dechiralization lines (parallel to $Ox$) in the $zy$ plane. Close to the surfaces the field is homogeneous. Between the lines the helix is wound. Thick arrows symbolize the antiparallel polar vectors defining the globally antiferroelectric character of the cell.

lobes are associated with the unwinding transition seen in permittivity measurements. On the other hand, the central lobe is associated with the low-field dielectric hysteresis described above in Fig. 2. In addition, we observe that the central lobe width increases with increasing frequencies.

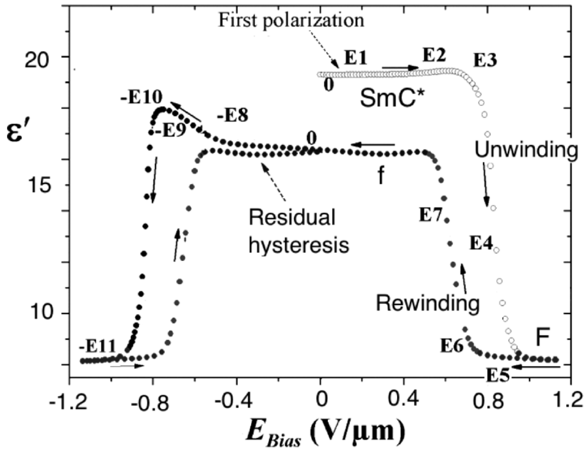

FIG. 2. Hysteresis cycle of the dielectric permittivity $\varepsilon'$ vs dc bias voltage $E_{\text{bias}}$ in a 7-$\mu$m-thick cell at 800 Hz. The phases (Sm$C$*), ferrielectric ($f$), and ferroelectric ($F$) are indicated. $E1$–$E11$ represent field values of the main characteristic points of the curve. They are interpreted at the dechiralization line scale in Fig. 9. The figure shows the difference between the first polarization curve ($E1-E3$) and the low-field part of the hysteresis curve ($E7$ to 0). The main hysteresis appears between $-E8$ and $-E11$, whereas the residual hysteresis is present between 0 and $-E8$. $-E10$ shows the anomalous maximum of permittivity.

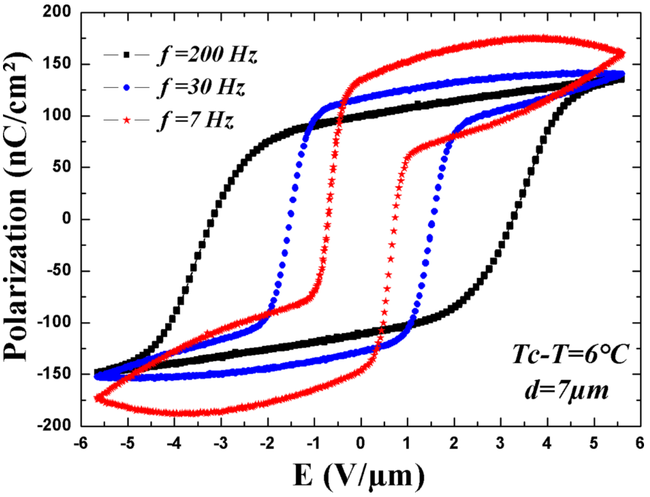

FIG. 3. Polarization versus electric field for different frequencies $f$.

All of these anomalies can be simply interpreted within *the ferrielectric scenario,* where macroscopic polarization occurs spontaneously beside the classical Sm$C$* helical polarization field. Thus, the two zero-field states observed in the sample, obtained in the first polarization curve and after cycling, respectively, correspond to distinct phases. The first one is the usual macroscopically nonpolarized Sm$C$* phase. The second one ($f$) is a polarized phase with ferrielectric properties. Moreover, at zero field, Sm$C$* is stable and $f$ is metastable. This assumption allows us to explain the observed anomalies: (i) the single low-field loop observed in permittivity and $P(E)$ cycles; (ii) the divergence (maximum) of the permittivity when the ferrielectric phase approaches its stability limits; and (iii) the difference of low-field permittivity between the first polarization curve (Sm$C$*) and the cycle ($f$). In the first polarization curve, the system stays in the stable Sm$C$* phase. Upon increasing field it undergoes a first-order transition at $E3$ (Fig. 2) toward an aligned ferroelectric phase with positive polarization ($F^+$) after the Sm$C$* helix unwinding. Upon decreasing field it undergoes a first-order rewinding transition at $E6 < E3$ toward a domain of the ferrielectric phase with positive polarization ($f^+$), which remains metastable up to zero field. At negative fields (–$E10$) this state undergoes a transition toward the $F^-$ domain with negative polarization.

During the field cycle, $-E_{\max} \rightarrow 0 \rightarrow +E_{\max} \rightarrow 0 \rightarrow -E_{\max} \ldots$, the following periodic phase sequence is predicted,

$$F^- \rightarrow f^- \rightarrow F^+ \rightarrow f^+ \rightarrow F^- \ldots,$$

so that the system is never of Sm$C$* phase character.

## II. PHENOMENOLOGICAL THEORY

In order to work out a phenomenological theory accounting for these anomalies, let us analyze the symmetry groups $G$ (zero field) and $G^E$ (under applied field) of the various phases involved in the reordering processes induced by the electric field. Their group-subgroup relationships are presented in Fig. 4(a). Let us first focus on the symmetries of bulk phases [the smectic layers and the helix axis are, respectively, normal and parallel to $Oy$, and the field is applied along $Oz$ (Fig. 1)]. The symbols 1D, 2D, and 3D indicate the number of dimensions where continuous translations are present in $G$ and $G^E$. The groups are written according to the international notation where, for instance, $P2\infty2$ means that the generators of the group are a continuous rotation axis parallel to $Oy$, and twofold axes parallel to $x$ and $z$. The notation $\infty_1$ means that the continuous rotations are replaced with continuous helical combinations of rotations with translations (in a similar way as $2_1$ means a twofold helical axis in standard space group notation). Note that at the micron scale considered in this

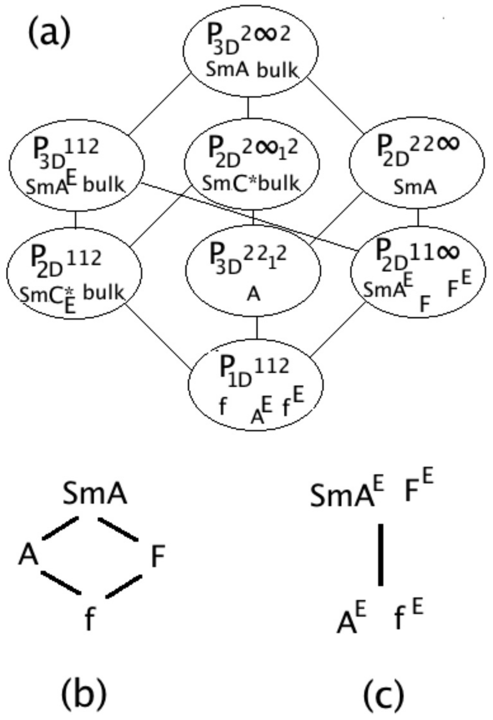

FIG. 4. (a) Group-subgroup relationships between the Sm*A*, Sm*C** (*A*), ferroelectric (*F*), and ferrielectric ($f$) phases, in the bulk and in the cell, with and without field. (b) Symmetry breakdown pattern in a cell at zero field. (c) Symmetry breakdown pattern in a cell under electric field.

work translation symmetries normal to smectic layers can be considered as continuous:

Sm*A*: $G_{A,\text{bulk}} = P_{3\text{D}}2\infty2$ (generated by 3D translations, continuous rotations $C_y$, and by twofold rotation axes parallel to the layers). Under electric field, it loses its continuous rotations and becomes

$$G^E_{A,\text{bulk}} = P_{3\text{D}}112.$$

Sm*C**: $G_{C,\text{bulk}} = P_{2\text{D}}2\infty_1 2$ (generated by continuous translations along $Ox$ and $Oz$, by continuous screw axes along $Oy$, and by twofold axes parallel to $x$ and $z$). Under electric field, the helical axis is broken into discrete translations along $Oy$, and the group loses its twofold axes, except $C_{2z}$:

$$G^E_{C,\text{bulk}} = P_{2\text{D}}112.$$

In a cell with planar geometry, the symmetries are broken by the cell walls ($\lambda$ is the helix pitch; that is, the distance between two neighboring dechiralization lines): All translations parallel to $Oz$ and all continuous rotations or screw axes parallel to $y$ are lost.

Sm*A*: $G_{\text{Sm}A} = P_{2\text{D}}22\infty$ (generated by continuous translations $t_x$ and $t_z$ parallel to the cell walls, by the continuous rotations $C_z$, and by the twofold axes $C_{2x}$ and $C_{2y}$). Under electric field,

$$G^E_{\text{Sm}A} = P_{2\text{D}}11\infty.$$

Sm*C**(*A*): $G_A = P_{1\text{D}}22_12$ (generated by $t_x$, $C_{2x}$, and $C_{2z}$, and the twofold screw axis $C_{2y}t_{y=1/2}$). Under electric field,

$$G^E_A = P_{1\text{D}}112.$$

Since $G_A$ is an antiferroelectric symmetry (the screw axis $2_1$ generates alternating polarization along $Oy$), we will hereafter denote this phase *A*. It should not be confused with traditional antiferroelectric liquid crystals where the antipolarization arises at the molecular level, while it arises in our system at the micron scale ($\lambda$):

Ferrielectric: $G_f = G^E_f = P_{1\text{D}}112$ (generated by $t_x$, discrete translations $t_{y=\lambda}$, and $C_{2z}$).

Ferroelectric: $G_F = G^E_F = P_{2D}11\infty$ (generated by $C_z$ and $t_x$, $t_z$).

In the cell the corresponding sequences of symmetry breakdowns [Figs. 4(b) and 4(c)] result from the onset of two order parameters [22], $\eta$ and $P$, representing the following: (i) $\eta = \varepsilon e^i\phi$, a transverse polarization (or tilt) wave $\mathbf{p}(y)$, with $p_x + ip_z = \eta e^{iky}$; and (ii) $P$, the $z$ component of the macroscopic polarization.

When an electric field $E$ is applied along $Oz$, the free energy $F$ depends on $E$, $P$, and the modulus $\rho$ of the complex wave amplitude $\eta$:

$$\begin{aligned} F = a\rho^2 + (c/2)\rho^4 + bP^2 + (d/2)P^4 \\ + (g/2)P^6 + K\rho^2P^2 - EP, \end{aligned} \tag{1}$$

where the phenomenological coefficients $a$,$c$,$b$,... depend on temperature. $F$ does not depend on the Goldstone angle $\phi$ because it must be invariant under the continuous translation symmetry along $Oy$ of the parent Sm*A* phase. A six-order expansion in $P$ with $d < 0$, $g > 0$ is necessary in order to account for the observed behavior. Indeed, an expansion restricted to the fourth order in $P$ does not allow a metastable ferrielectric phase at zero field.

We note that, although Eq. (1) includes only homogeneous terms (without derivatives), it yields the stabilization of inhomogeneous (helical) structures since the primary order parameter $\eta$ is the complex amplitude of a circularly polarized polarization (or tilt) wave (see Ref. [23] for details of the method) instead of the local polarization (or tilt) used in the standard Landau approach to ferroelectric liquid crystals. The onset of the order parameter below the critical temperature yields full wave condensation, i.e., a helical structure with finite pitch. Additional (Lifshitz and Ginzburg) gradient terms would only permit temperature or field variations of the pitch, which are not observed in CFL08 for reasons detailed in Ref. [20] and briefly discussed below. The equations of state,

$$\begin{aligned} a\rho + c\rho^3 + K\rho P^2 = 0, \\ 2bP + 2dP^3 + 3gP^5 + 2K\rho^2 P = E, \end{aligned} \tag{2}$$

yield at zero field the phase diagram presented in Fig. 5.

In addition to Sm*A*($\rho = P = 0$), *A* ($\rho \neq 0$, $P = 0$), and $f(\rho \neq 0, P \neq 0)$, a virtual globally ferroelectric phase *F* (not to be confused with the locally ferroelectric, but actually antiferroelectric, *A* phase): $\rho = 0$, $P \neq 0$ is stabilized. Upon varying the temperature the system follows a thermodynamic path (denoted $c$ in Fig. 5) that cannot cross the *F* stability domain. At low temperature the stable *A* phase coexists with the metastable $f$ phase. Above $T_1$, $f$ becomes unstable and the conventional situation is restored.

Under small constant applied field, the previous phase diagram is only slightly modified. The symmetry difference between Sm*A* and *F*, and the difference between *A* and $f$,

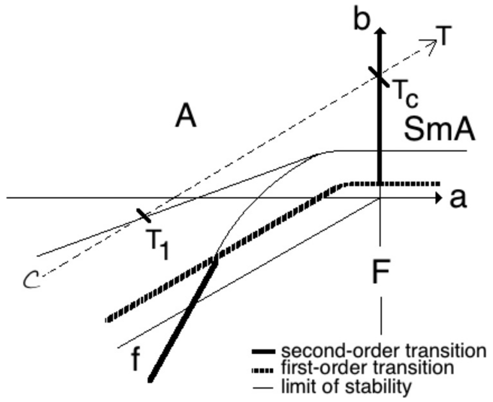

FIG. 5. Zero-field phase diagram of the ferrielectric model. Dotted lines represent first-order transitions. Thick solid lines represent second-order transitions. Thin lines represent the stability limits of the stable phases: Sm$A$, $A$ (SmC*), ferrielectric $f$, and ferroelectric $F$. The dotted line indicates the thermodynamic path followed by the system when temperature is varied. At low temperature (below $T_1$) the $A$ phase remains stable but coexists with the metastable $f$ phase.

disappear [see Fig. 4(c)] so that the corresponding first-order transition in Fig. 5 becomes isostructural.

The temperature-field phase diagram along the thermodynamic path $c$ is presented in Fig. 6(a). For fixed temperatures, the corresponding hysteresis $P(E)$ curves are presented in Fig. 6(b).

Just below $T_c$, only $A$ is stable and no hysteresis can be observed in the $P(E)$ curves. Between $T_1$ and $T_2$ a standard double hysteresis is predicted. Between $T_2$ and $T_3$ the system has one stable state, $A$, and two metastable states, $f^+$ and $f^-$, at zero field. Starting from $A$, upon increasing field (first polarization curve) the system undergoes a first-order transition to $f^+$, and then a second-order transition to $F^+$. Upon decreasing field, it undergoes a rewinding transition and remains in phase $f^+$ down to zero field, where it exhibits remnant polarization. We note that the first polarization curve should be distinguished from that observed in a solid ferroelectric, which is formed by a collection of oppositely polarized domains of the spontaneously polar phase. Similarly, in solids the remnant polarization arises in single domains of the zero-field stable phase, while in our model it occurs in the metastable $f$ phase.

We have seen that between $T2$ and $T3$ the $P(E)$ hysteresis curve has dual character: a single loop at weak fields and a double loop at high fields, which coincides with the observed behavior (see Fig. 3) except for one point; namely, a two-step transition is predicted from $A$ to $F$, one at $E_c$ and the other at $E_3$, whereas observations show a single-step transition.

Accordingly, one has to refine the model in order to obtain $E_c < E_3$. This can be achieved by letting the thermodynamic path cross the stability limit of $F$ in Fig. 5 twice. The $P(E)$ hysteresis curve then becomes as shown in Fig. 7(a). The cycle overlaps a double-loop hysteresis at strong fields, characteristic of helielectric states, and a single loop at low fields, characteristic of ferroelectrics. The corresponding static permittivity hysteresis cycle $\varepsilon'(E)$ is presented in Fig. 7(b).

In fact, when upon decreasing field the cycle approaches the field $-E_2$, the system is in the domain $f^+$ of positive polarization of the ferrielectric phase. At $-E_2$ this state becomes unstable and the system can undergo a transition either toward the stable $A$ phase, as is assumed in Figs. 7(a)

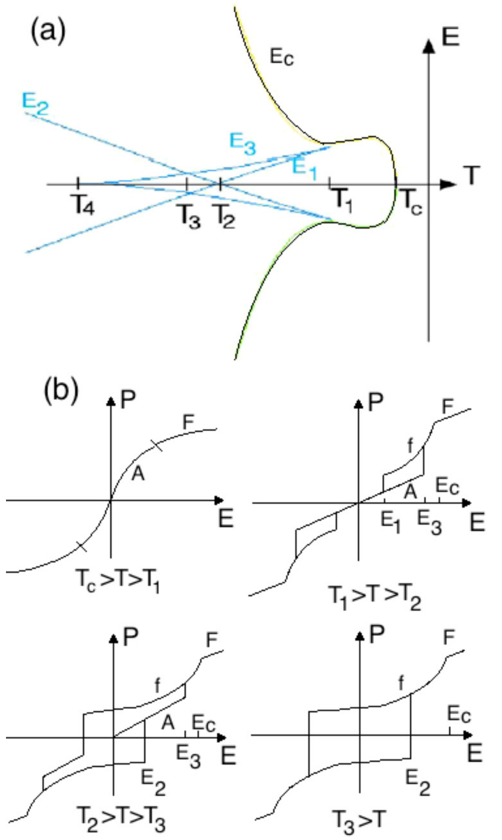

FIG. 6. (a) Temperature-field phase diagram along the thermodynamic path. The thin lines indicate the limits of stability of the various stable or metastable phases. (b) Polarization ($P$) vs applied field ($E$) hysteresis cycles at different fixed temperatures.

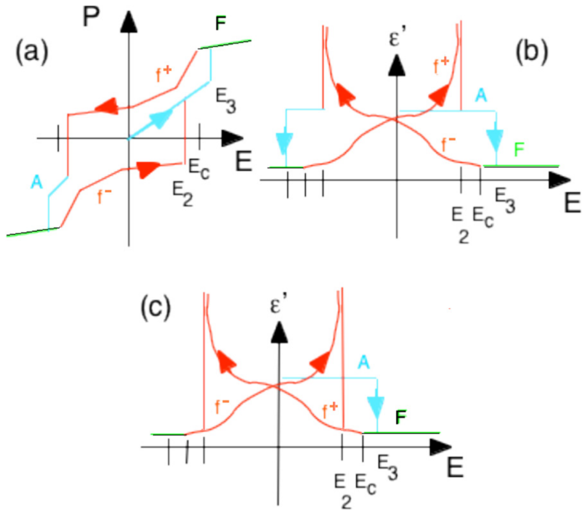

FIG. 7. (a) Polarization-field $P(E)$ cycles inn the first scenario: transition $f^+ \rightarrow A$ at $-E2$. (b) Permittivity-field $\varepsilon'(E)$ cycle in the first scenario. (c) $\varepsilon'(E)$ in the second scenario: transition $f^+ \rightarrow f^-$ at $-E2$.

and 7(b), or toward the metastable domain $f^-$ with negative polarization, yielding the cycle $\epsilon'(E)$ shown in Fig. 7(c). In this scenario only the single low-field loop is predicted, in agreement with observations of $P(E)$ curves above 60 Hz (Fig. 3).

The permittivity cycle shown in Fig. 7(c) is also in good agreement with experimental curves shown, for instance, in Fig. 2. Indeed, one observes low-field hysteresis, as well as different behaviors between the cycle and the first polarization curve and one maximum of $\varepsilon'$ before the unwinding transition in the cycle. The divergence of $\varepsilon'$ predicted in Figs. 7(b) and 7(c) occurs at the stability limit of the $f$ phase upon increasing field. In fact, since the transition is first order, it can occur before the limit $E_2$ is actually reached, and the divergence should turn into a simple sharp maximum at $E < E_2$, as shown in Fig. 2.

As is usual with Landau-type approaches to phase transition phenomena, the free energy expansion exhibits very general features determined only by symmetry considerations, adapted to a wide class of materials. However, the choice of the coefficient signs and maximum powers in Eq. (1), together with the thermodynamic path depicted in Fig. 5, are specifically adapted to account for the anomalies observed in CFL08.

The choice of destination of the transition is a more complex issue than the establishment of phase diagrams, because it also involves the dynamics of the system far from equilibrium. We will not attempt to deal with this difficult problem, and will simply suggest the following heuristic description: When the field is cycled at small speed, the system goes from $f^+$ to the actually stable phase $A$, leading to a double-loop $P(E)$ curve. At high frequencies, on the other hand, the system transits from $f^+$ to $f^-$ and a single loop is generated. The concomitant decrease in the width of the single loop upon increasing frequency can be explained by the first-order nature of the transition at $E_2$: As stated above, this type of transition can occur actually at any field between $E = 0$ and the *superheating* field $E_2$ corresponding to the metastable limit of $f^+$. The actual value of the transition field depends on defects and dynamics. We therefore assume that at high speed the real transition field goes away from $E_2$, yielding the observed shortening of the single-loop $P(E)$ width (Fig. 3) [17,18]. All of the observed qualitative anomalies listed in the Introduction are thus well accounted for within our model.

## III. LIMIT PHASES AND DECHIRALIZATION LINES

The theory presented in Sec. II is mainly based on symmetry considerations. Our analysis of the singularities has thus a large domain of validity, independent of any interpretative model and of any specific material. Our interpretation of the primary order parameter $\eta$ as a vector wave amplitude does not modify these predictions. However, this interpretation is, in fact, valid only when conditions are fulfilled by the experimental cell. Indeed, the cell is a complex system made of charged and/or polarized electrically interacting objects: helix, walls, and dechiralization lines. In Ref. [20] we have analyzed the effects of these interactions on the stable structures, and we show that in two limit cases the situation can be simplified: (i) For thick cells the helix dominates, and (ii) for thin cells the lines dominate the field-induced transition (unwinding) mechanism. We have also shown that in the thickness range (3–15 $\mu$m) studied in this work, the line-dominated regime applies. A new interpretation of the order parameters is thus needed. We note that it will not alter the validity of the main results presented in the preceding section (nature and behavior of the singularities). We will see, however, that it yields an enrichment of the predictions, particularly of the list of possible stable phases and transitions.

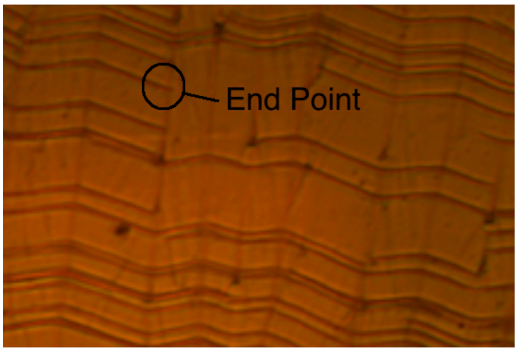

FIG. 8. Sample surface under crossed analyzer and polarizer in a 15-$\mu$m-thick sample. The dechiralization lines appear as horizontal broken parallel dark stripes. The end point of one line (where it leaves the liquid crystal normal to the figure) is indicated.

Theoretically, the field-induced unwinding transition in the bulk can be second order. It happens, then, after continuous vanishing of the helix wave vector $k = 2\pi/\lambda$. In contrast, in a thin sample we observe that $\lambda$ remains almost constant close to the transition, and the unwinding results from the migration of the dechiralization lines toward one of the sample walls, followed by their exit out of the liquid crystal [20]. Indeed, the dechiralization lines are submitted to Coulomb forces in the direction of the field. Analogously, the rewinding transition results from the entrance and inverse migration of the lines. This process is clearly evidenced in our samples, where one can observe under a microscope the entrance and exit of each line individually, which appears as a dark stripe on the observed surface. The exit begins at one point of the surface cell (Fig. 8) where the line meets a structural defect (for instance, a focal conic domain), and one then sees the end point of the line moving along the line until it completely disappears. A more detailed analysis of this interpretation of the broken lines observed in Fig. 8 is available in Ref. [20], together with a dynamical model. We will not discuss out-of-equilibrium phenomena any further in the present work, and will consider only equilibrium unbroken lines in the theory.

Observations of line motion follow precisely the hysteretic dielectric behavior described in Sec. II. The optic observations are schematically summarized in Fig. 9. At zero field just after cooling the lines are symmetrically located with respect to the central plane of the sample and the system is in phase $A$. No stripe is then observed. We denote by $H$ the upper lines and by $D$ the lower lines. Upon increasing field the lines move toward the field direction and $H$ lines become visible before eventually leaving the sample. Finally, $D$ lines go out of the sample, leaving a homogeneous texture at maximum field. Upon decreasing field the lines again come inside the sample, but stay in an unsymmetrical state when zero field

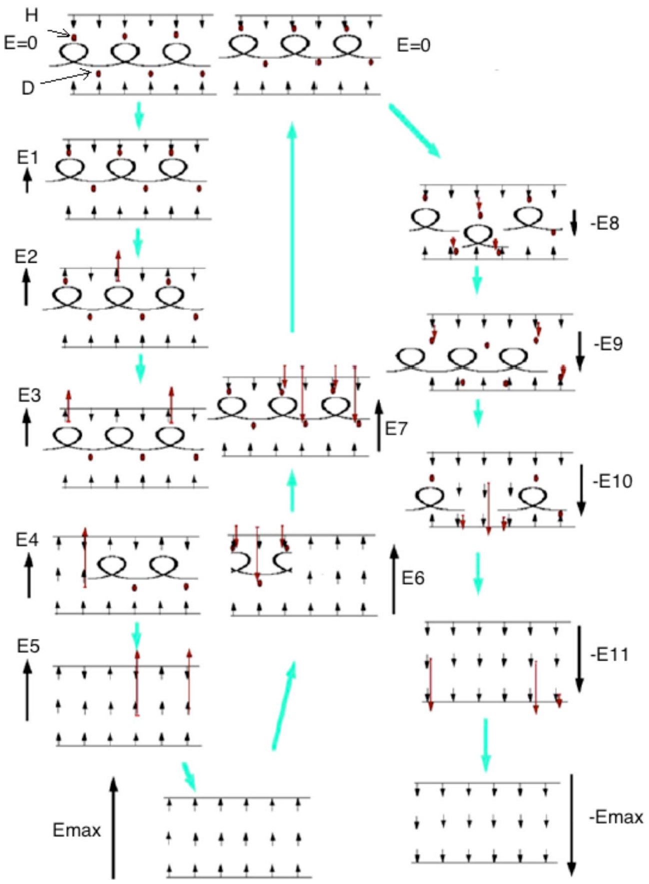

FIG. 9. Schemes of the migration of the dechiralization lines during field cycling, as observed at $T_C - T = 5\,^\circ\mathrm{C}$ in a 15-$\mu$m-thick sample from $E = 0$ to $E_{\max} = 1\ \mathrm{V}/\mu\mathrm{m}$. Schemes in the first column represent the cell during the first polarization curve. The second and third rows represent one-half of one cycle. The field values $E1$, $E2$, ... are defined in Fig. 2. Small arrows represent the polarization field. Large arrows show the displacements of the lines submitted to Coulomb forces. A wrapped line indicates the presence of the helix. $H$ and $D(E = 0)$ represent the upper and lower line lattices, respectively.

is reached. The system is then in the $f^+$ state with a positive internal field pushing $D$ lines toward the surface and deforming their structure, making them visible under a microscope. Upon resuming field cycling, the exit and entrance line behavior occurs without any new stabilization of $A$. We observe that the texture of the sample is different, upon increasing and decreasing fields, respectively, even at small fields. Thus, optic measurements exhibit anomalies similar to those observed in dielectric experiments: remnant zero-field polarization and small-field hysteresis.

Note that one fact remains unexplained: During the first polarization curve one does not observe any stripe while the system is in the $A$ phase; lines should therefore be present. We have no satisfactory arguments to account for the observed absence of lines, and thus we must speculate that a line can only be seen under a microscope when it "feels" an electric field (applied or internal): The field modifies the line structure and brings it closer to the surface, which would make it visible between the crossed analyzer and polarizer.

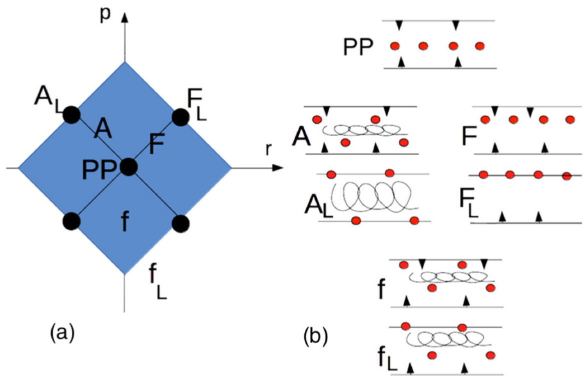

FIG. 10. (a) Order-parameter space. The parent phase (PP) lies at the center of the square, with $A$ and $F$ on the diagonals. The gray area corresponds to the normal ferrielectric f phase. The limit phase $f_L$ lies on the square boundaries. $A_L$ and $F_L$ are represented by dots located on the boundaries. (b) Dechiralization line lattices in normal and limit phases. Parts of the sample where the helix is unwound are represented by dark arrows indicating the polarization direction; wrapped thin solid lines represent the wound helix.

We now translate the theory introduced in Sec. II in terms of line motions. In the preceding section, the order parameters $\rho$ and $P$ are formally defined by their transformation properties with respect to the Sm$A$ symmetry group, and then related to the molecular polarization field. They can be given different meanings when considering the transitions as resulting from the dechiralization line motion. However, this interpretation requires a change in the definition of the parent phase (PP), since in Sm$A$ no dechiralization lines exist. The parent high-symmetry phase is now defined as the locally polarized state where all the lines are located on the sample central plane ($z = 0$). Their distance is then $\lambda/2$ since the corresponding lattice merges both $H$ and $D$ lines [see Fig. 10(b)]. The symmetry group is $P_{1\mathrm{D}}222$ characterized by discrete translations $t_{y=\lambda/2}$.

Thus, in the ordered phases $A$, $F$, and $f$ the lines move away from the center. Half of the lines ($H$) move up while the other half ($D$) move down, leaving a space to the helix for winding. Denoting the distance of the $i$th line with respect to the center as $z_i$, one can write

$$z_i = p + (-1)^i r, \tag{3}$$

which defines the new order parameters $p$ and $r$ with the same symmetry as $P$ and $\rho$. We note that due to the discrete translation symmetry of the parent phase along $Oy$, no Goldstone angle $\phi$ is now present in the description. The lattices of the lines are represented in Fig. 10(b) for each stable phase: PP, $A$, $F$, and $f$.

The free energy and equations of state given in Eqs. (1) and (2) remain valid (after replacing $P$ by $p$ and $\rho$ by $r$). However, an important difference from the previous model results from the fact that the values of $p$ and $r$ are now constrained to stay within the square domain shown in Fig. 10(a). Indeed, when lines reach sample walls—that is, for $z_i = p \pm r = \pm L/2$—then $p$ and $r$ reach the boundaries of this square.

New *limit phases* can thus be stabilized: $A_L$, $F_L$, and $f_L$, located at the square boundaries. The structure of their line patterns is presented in Fig. 10(b). The existence of such limit

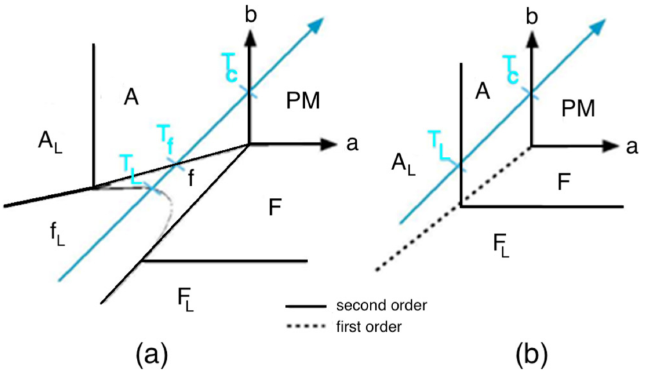

FIG. 11. Zero-field phase diagrams. (a) $K^2 < cd$ and (b) $K^2 > cd$. Arrows indicate possible thermodynamic paths.

phases is an unconventional feature of Landau theory arising when the order parameter belongs to a bounded domain. It is remarkable that, despite the absence of symmetry breakdown between normal and limit phases, the latter have extended stability domains in the phase diagram, and second-order transitions are permitted with their normal analogs.

We note that the disposition of the lines after they reach the sample walls is still controversial. In a classical view of defects in condensed matter, they completely disappear and the polarization field remains perfectly aligned everywhere in the sample. In contrast, Pavel *et al.* have proposed that a residue persists on the walls, consisting of half-integer defects corresponding to $\pi$ disclinations [10].

Two theoretical phase diagrams are presented in Fig. 11 for $g = 0$ and $d > 0$. When $K^2 < cd$ only second-order transitions are present, between either group and/or subgroup related phases, or between normal phases and their limit analogs. When $K^2 > cd$ first-order transitions take place between both normal and limit $A$ and $F$ phases.

We now identify the states observed in Fig. 9:

(i) During the first polarization process : $A$ is stable at zero field. It becomes $f$ between $E0$ and $E1$. Between $E1$ and $E2$ the exit of $H$ lines transforms the sample into $f_L$. Between $E4$ and $E5$ the helix unwinding resulting from the exit of $D$ lines stabilizes $F_L$.

(ii) During the cycling process: Between 0 and $E8$ the system is ferrielectric $f^+$. Between $E8$ and $E9$ it undergoes a transition from $f^+$ to $f^-$. Between $E10$ and $E11$ the helix is unwound and all the lines go out of the cell, which persists in $F_L$ up to $E_{\text{max}}$.

(iii) When the field decreases down to $E6$, the lines $H$ and $D$ penetrate into the cell simultaneously. Between $E6$ and $E7$ the helix is wound and the cell becomes $f^+$ down to zero field.

One sees that during the whole process the system goes through the phases $A$, $F_L$, $f$, and $f_L$, but never through $A_L$ or $F$.

We note that the lines model presented remains at an elementary theoretical level. We will not develop it further, and we use it mainly to get useful, though essentially qualitative, predictions concerning the list of stable phases and the nature of the corresponding transitions. The macroscopic polarization $P$ can be considered a secondary order parameter controlling the dielectric properties of the cell. Since it is linearly coupled to $p$, it exhibits exactly the same qualitative properties as $p$, and it presents the same singular behaviors in the $A$, $F$, and $f$ phases described in the preceding sections. We will not work out the dielectric modifications appearing close to the limit-phase transitions in this paper. More quantitative results about line interactions, critical field values, and thickness behavior dependence can be found in Ref. [20]. However, these results, in which the unwinding transition is analyzed with respect to the line characteristics, and particularly to the complex behavior of their electric charges, did not permit us to relate this analysis quantitatively to the onset of ferrielectricity. Nevertheless, the line interaction model [20] permits us to determine the actual pitch value, i.e., the interline distance, which results from a compromise between repulsive interline forces, electric neutrality, and winding bulk effects, together with line charge variations.

## IV. CONCLUSIONS

We interpret the dielectric and optic anomalies observed in the CLF08 Sm$C^*$ phase below the ordering transition temperature as resulting from the existence of a metastable ferrielectric phase in addition to the usual $A$ phase (confined Sm$C^*$). The tristability $(A, f^+, f^-)$ of the system under an electric field then accounts directly for these anomalies. The helielectric Sm$C^*$ state is made actually antiferroelectric by the symmetry breaking effects of the sample geometry. The ferrielectric phase results from the spontaneous onset of a macroscopic polarization in the material. Since such a polarization is forbidden by chirality at molecular scale, it necessarily takes its origin from mesoscopic microstructures, the dechiralization lines, produced by the unwinding effect of sample surfaces. The spontaneous polarization arising at the corresponding micron scale ($\lambda$) is automatically unwound by the surface effects in samples a few $\mu$m thick.

The main effects of the presence of the ferrielectric state, namely low-field hysteresis and remnant polarization, are visible in dielectric measurements as well as under a microscope. Indeed, the charged dechiralization lines interact with the induced internal field and are compelled to follow its hysteretic behavior. However, the converse process is also possible: The existence of spontaneous breakdown of the lines' lattice symmetry at zero field stabilizes a structure with a ferrielectric group at the micron scale. The dielectric effects then result from the coupling of the polarization field with the lines' lattice. We expect this line-based mechanism to yield ferrielectricity in thin samples where surface effects are dominant. This interpretation is supported by the fact that the observed unwinding transition occurs without any observable change in the line lattice spacing (i.e., the helix pitch $\lambda$), which means the helix-field interactions are not dominant in the unwinding process. Coulomb forces acting on the lines are responsible for their migration across the sample and their exit after the elastic barrier is overcome. We assume that the same forces (elastic and electric) between lines and cell walls are responsible for the onset of ferrielectricity in this material.

This theoretical model is consistent and accounts for all of the anomalous effects observed in dielectric and optic experiments on CLF08. However, a few points remain to be clarified: (i) Why are dechiralization lines not visible at zero field in the first-polarization curve? (ii) What are the electric effects of the ions produced by the strong chemical instability of this material? More specifically, can the electric effects also explain the observed anomalies? (iii) Are the observed stripes really traces of the dechiralization lines?

---

[1] R. B. Meyer, L. Liebert, L. Strzelecki, and P. Keller, J. Phys. Lett. **36**, 69 (1975).

[2] P.-G. de Gennes, Rev. Mod. Phys. **64**, 645 (1992).

[3] S. Garoff and R. B. Meyer, Phys. Rev. Lett. **38**, 848 (1977).

[4] P. Oswald and P. Pieranski, *Les cristaux liquides: Concepts et propriétés physiques illustrés par des expériences* (Gordon and Breach, Paris, 2002), Vol. 1.

[5] R. B. Meyer, Mol. Cryst. Liq. Cryst. **40**, 33 (1977).

[6] H. R. Brand, P. E. Cladis, and P. L. Finn, Phys. Rev. A **31**, 361 (1985); S. T. Lagerwall, *Ferroelectric and Antiferroelectric Liquid Crystals* (Wiley, New York, 2008).

[7] Y. Bouligand and M. Kleman, J. Phys. (Paris) **40**, 79 (1979).

[8] M. Brunet and P. Martinot-Lagarde, J. Phys. II **6**, 39 (1996); M. Brunet and O. Parodi, J. Phys. (Paris) **43**, 515 (1982).

[9] M. V. Kurik and O. D. Lavrentovich, Sov. Phys. Usp. **31**, 196 (1988).

[10] V. Bourny, J. Pavel, P. Gisse, and H. T. Nguyen, Ferroelectrics **241**, 247 (2000).

[11] T. Soltani, A. Gharbi, J. P. Marcerou, and S. Gineste, Eur. Phys. J. Appl. Phys. **55**, 10201 (2011).

[12] F. Ghoddoussi, M. A. Pantea, P. H. Keyes, R. Naik, and P. P. Vaishnava, Phys. Rev. E **68**, 051706 (2003).

[13] J. Hemine, A. Daoudi, C. Legrand, N. Isaert, A. El kaaouachi, and H. T. Nguyen, Physica B **399**, 60 (2007).

[14] J. Lagerwall, P. Rudquist, S. Lagerwall, and B. Stebler, Ferroelectrics **277**, 239 (2002).

[15] A. Mukherjee, M. Rahman, S. S. Bhattacharyya, A. Yoshizawa, and B. K. Chaudhuri, Chem. Phys. Lett. **45**, 7315 (2008).

[16] V. Bourny and H. Orihara, Phys. Rev. E **63**, 021703 (2001).

[17] H. P. Logbo, Doctoral thesis, University of Picardie, France, 2013.

[18] H. P. Logbo, Y. Gagou, R. Dabrowski, M. Zurowska, and B. Mettout, Liq. Cryst. **43**, 639 (2016).

[19] J. Dziaduszek, R. Dąbrowski, K. Czupryński, and N. Bennis, Ferroelectrics **343**, 3 (2006).

[20] B. Mettout, H. P. Logbo, H. Vasseur, and P. Gisse, Liq. Cryst. (2016).

[21] M. E. Lines and A. M. Glass, *Principles and Applications of Ferroelectrics and Related Materials* (Clarendon, Oxford, UK, 1977).

[22] V. L. Lorman, A. A. Bulbitch, and P. Tolédano, Phys. Rev. E **49**, 1367 (1994).

[23] V. L. Lorman and B.Mettout, Phys. Rev. Lett. **82**, 940 (1999); Phys. Rev. E **69**, 061710 (2004); B. Mettout, *ibid.* **75**, 011706 (2007).